

Characterization and optimization features of high-efficiency silicon solar cells with dominating surface recombination

A.V. Sachenko^{1*}, V.P. Kostylov^{1*}, I.O. Sokolovsky¹, and A.I. Shkrebtii²

¹*V. Lashkaryov Institute of Semiconductor Physics, NAS of Ukraine, 41 Nauky Ave., 03028 Kyiv, Ukraine*

²*Faculty of Science, Ontario Tech University, 2000 Simcoe Street North, Oshawa, ON, L1G 0C5 Canada*

*Corresponding author e-mail: avsacenko@gmail.com, vkost@isp.kiev.ua

Abstract. This work investigates the features of modeling photoconversion processes in highly efficient solar cells based on silicon single crystal, where the contribution of surface recombination significantly prevails over the contributions of recombination in the space charge region (SCR) and non-radiative excitonic recombination involving impurity centers. It is shown that in this case, the key characteristics of the photoconversion process, namely the dark and light current-voltage characteristics and the dependences of the output power of SC, obtained with account of recombination in the SCR and non-radiative excitonic recombination involving impurity centers, practically coincide with each other. The results of modeling were compared with the experiment for the SC from two works, where the above-mentioned conditions occur. The analysis confirmed the consistency of the theoretical dependences obtained with and without account recombination in the SCR and non-radiative exciton recombination with the experimental data. It is shown that optimizing the base doping level and thickness of the studied SC causes an increase in its efficiency from 24.37% to 24.62%. The results obtained in this work allow to explain why previously the recombination in the SCR was not taken into account in the theoretical modeling of the characteristics of the SC based on silicon single crystal in the overwhelming number of works, and also to show that the general approach is valid in the case of any ratio between the components of the recombination currents in single-crystalline silicon.

Keywords: modeling, silicon solar cell, surface recombination rate, recombination in SCR, photoconversion efficiency.

<https://doi.org/10.15407/spqeo28.03.351>

PACS 72.20.J, 78.60.J, 88.40.jj

Manuscript received 19.05.25; revised version received 02.08.25; accepted for publication 03.09.25; published online 24.09.25.

1. Introduction

The reviews [1–4] analyzed the state of investigations and prospects for photovoltaic applications. These investigations are focused on highly efficient solar cells (SCs) based on monocrystalline silicon, with account of 97% of their production [5].

Since the record efficiency of silicon SCs (27.3%) [6] became close to the theoretical limit (29.6%) [7–9], the importance of an adequate model for accurate simulation and optimization of their characteristics is increasing. The theoretical approach in [10] allows for the correct modeling of the experimental dependences of the key photovoltaic characteristics of the mentioned SCs. This approach considers the following recombination mechanisms in monocrystalline silicon. These are radiative recombination, interband Auger recombination, surface recombination, bulk Shockley–Reed–Hall (SRH) recombination, space charge region (SCR) recombination, and non-radiative excitonic recombination by the

Auger mechanism *via* deep impurity level. The last two mechanisms are not considered in existing works on modeling the characteristics of silicon SCs, except for our previous works. This work explains when this can be done. The specified neglect is valid when the SCR recombination and non-radiative excitonic recombination are significantly smaller than the surface recombination.

In this work, we theoretically modelled the key photoelectric and optical characteristics for the SCs obtained in [11] for the first time. SCs developed in this work are designed according to the so-called IBC scheme with back contacts and separated p^+ - n and isotype n - n^+ barriers.

The modeling approach developed in [10] was used for their modeling characterization. The analysis was performed using six and four processes describing recombination in the SC base region. In four processes, the mechanisms of SRH recombination, surface recombination, interband Auger recombination, and radiative recombination were considered. When considering six processes, recombination in the SCR and non-radiative

excitonic recombination by the impurity Auger mechanism were additionally included.

It was shown in [10] that when the recombination in the SCR exceeds the surface recombination [12–16], the approximation of six recombination processes better describes the experimental characteristics of the SC than the approximation of four recombination processes. Particularly, large differences in these cases are observed when calculating an effective lifetime in the base region, which depends on the excess concentration of electron-hole pairs. In the studied SCs, the surface recombination significantly exceeds the recombination in SCR. Therefore, both approximations give the same result, as will be shown below.

Another feature revealed in the analysis of the experimental results presented in [11] is a weaker-than-usual dependence of the surface recombination rate $S(\Delta n)$ on the excess concentration of electron-hole pairs. In the general case, the rate can be described as

$$S(\Delta n) = S_0 \left(1 + \frac{\Delta n}{n_0} \right)^r, \quad (1)$$

where S_0 is the initial surface recombination rate, n_0 is the equilibrium electron concentration in the base, and r is the slope of the $S(\Delta n)$ dependence. Usually, for most silicon SCs, the value r is 1, but in this case, $r = 0.62$. As will be shown below, r values less than 1 are realized when the charge in the SCR of the n^+ layer of the isotype $n-n^+$ junctions is smaller than the charge of the p^+ area.

It should be noted that despite the sufficiently high surface recombination rate, the efficiency of 24.37% in this SC is quite high. It can be explained by the small charge value of SCR of the n^+ -region, which results in a lower surface recombination rate at the maximum power point than at $r = 1$.

The second reason is the efficient light capture due to high-quality front surface texturing, which is evidenced by the spectral dependence of the external quantum efficiency $EQE(\lambda)$ and a high short-circuit current density (41.95 mA/cm²). All the above compensate for the relatively small open-circuit voltage.

In this work we calculate the light $J-V$ characteristics and the dependences of the output power P on the applied voltage, experimentally obtained in [17], using approximations of six and four-recombination mechanisms and ascertained that they visually coincide. We have already calculated the light $J-V$ characteristics obtained in [17], in the approximation of six recombination mechanisms. The calculation results were published in our work [18], but the calculation in the approximation of four recombination mechanisms was not carried out. It should be noted that [17] was published earlier than [11] and it considered the SCs with flat surfaces. Both works were carried out by the same research group. The main goal of our work [18] was to analyze the wavelength-dependent External Quantum Efficiency $EQE(\lambda)$ and Internal Quantum Efficiency $IQE(\lambda)$ for a flat SC with a flat surface in the general and limiting cases of large diffusion lengths compared to the thickness of the base.

We derived the corresponding expressions in [18] and established that the aforementioned limiting case of large diffusion lengths compared to the substrate thickness appears in [17].

In this work we calculated the recombination rate in SCR when the inverse lifetime in the SCR is described by a Gaussian. This part of the work is based on the theoretical approach proposed in [18]. The work is structured so that we first interpret the results obtained in [11], and only then analyze the experimental light $J-V$ characteristics and the applied voltage-dependent output power, obtained in [17] in the approximation of six- and four-recombination mechanisms.

2. Calculation of external quantum efficiency and short circuit current

The peculiarities of the theoretical approach, described in [10], that allows modeling the short circuit current J_{SC} , having $EQE(\lambda)$ dependences for the device structure, are the following. The analysis of the $EQE(\lambda)$ experimental dependence in SC samples of different thicknesses [15, 19] has shown that it can be divided into two regions. In the short-wave region ($\lambda < 800$ nm), denoted by the index s , the external quantum efficiency $EQE_s(\lambda)$ is practically independent of the sample thickness d . In the long-wave region ($\lambda > 800$ nm), denoted by the index l , a certain dependence occurs. In the long-wave region near the absorption edge, a modified Lambertian is used to calculate the external quantum efficiency in the following form:

$$EQE_l(\lambda, d) = \frac{f}{1 + b(4n_{Si}^2(\lambda)\alpha(\lambda)d)^{-1}}, \quad (2)$$

where the fitting non-dimensional parameter b determines the shape of the EQE_l dependence and describes the ratio of the photon mean path length in SC with ideal Lambertian surfaces to its actual mean photon path length, n_{Si} is the refraction index and $\alpha(\lambda)$ is the absorption coefficient of silicon, d is the SC thickness. The parameter f is chosen so that the values of EQE_s and EQE_l coincide at $\lambda = 800$ nm. It is worth noting that when $b = f = 1$, expression (1) turns into the well-known formula for the absorption capacity of SC, introduced in [20].

In the region $\lambda < 800$ nm, the experimental $EQE_s(\lambda)$ does not depend on the base thickness and is determined only by the losses due to reflection, shadowing, and absorption of light outside the base SC region.

By dividing the value $EQE(\lambda)$ into two components, we can calculate the dependence $J_{sc}(d, b)$:

$$J_{SC}(d, b) = q \left[\int_{\lambda_0}^{800} I(\lambda) EQE_s(\lambda) d\lambda + \int_{800}^{1200} I(\lambda) EQE_l(\lambda, b) d\lambda \right]. \quad (3)$$

Here, $I(\lambda)$ is the spectral density of the photon flux under AM1.5 conditions.

Fig. 1 shows the experimental dependences of the external quantum efficiency of SC obtained in [11]. One can see that the theoretical and experimental curves agree with each other at $b = 2.6$ and $f = 0.973$.

Using the expressions (2) and (3), we calculated the dependence of the short-circuit current of the SC from work [11] on the base thickness d , as shown in Fig. 2.

3. Dependences of the effective lifetime on excess concentration

We will describe below the algorithm for determining the experimental values of the total recombination rate in SCR, namely, the values of the recombination rate in SCR (S_{SCR}) and in the part of SCR that becomes neutral due to the reduction in band bending upon illumination, as proposed in [11]. The experimental S_{SCR}^{\exp} value is found using the expression:

$$S_{SCR}^{\exp} = d \left(\frac{1}{\tau_{eff}^{\exp}} - \frac{1}{\tau_{eff}^k} \right), \quad (4)$$

where d is the SC base thickness, τ_{eff}^k is an effective lifetime without the component describing the recombination time in SCR. This effective lifetime can be found from the following expression:

$$\tau_{eff}^k = \left(\frac{1}{\tau_{SRH}} + \frac{1}{\tau_{ex}} + \frac{1}{\tau_s} + \frac{1}{\tau_{Auger}} + \frac{1}{\tau_{rad}} \right)^{-1}, \quad (5)$$

where τ_{SRH} is the SRH recombination lifetime, τ_{ex} is the non-radiative exciton recombination lifetime, τ_s is the surface recombination lifetime, τ_{Auger} is the interband Auger recombination lifetime and, τ_{rad} is the radiative recombination lifetime.

The theoretical value S_{SCR}^{th} is found from the expression

$$S_{SCR}^{th} = S_{SCR}(\Delta) + \left(\frac{w(\Delta n=0) - w(\Delta n)}{\tau_R} \right) \frac{(n_0 + \Delta n)}{(n_0 + \Delta n) + b_R \Delta n}, \quad (6)$$

where

$$S_{SCR}(\Delta n) = \int_{y_w}^{y_0} \frac{(n_0 + \Delta n) dx}{\left[\left((n_0 + \Delta n)e^y + n_i(T) \exp\left(\frac{E_t}{kT}\right) \right) + b_r \left((p_0 + \Delta n)e^{-y} + n_i(T) \exp\left(-\frac{E_t}{kT}\right) \right) \right] \tau_R} F \quad (7)$$

$$F = \frac{L_D}{\left[(1 + \Delta n/n_0)(e^y - 1) + y_m + \left(\frac{p_0}{n_0} + \Delta n/n_0 \right) (e^{-y} - 1) \right]^{1/2}}, \quad (8)$$

$$w = \int_{y_0}^{y_w} \frac{L_D}{\left[\left(1 + \frac{\Delta n}{n_0} \right) (e^y - 1) - y + \frac{\Delta n}{n_0} (e^{-y} - 1) \right]^{0.5}} dy. \quad (9)$$

Here, τ_R is the lifetime in SCR, $b_r = C_{ps}/C_{ns}$, C_{ps} , C_{ns} are the coefficients of hole and electron capture by the recombination center, respectively, y – dimensionless potential, n_i – concentration of intrinsic charge carriers,

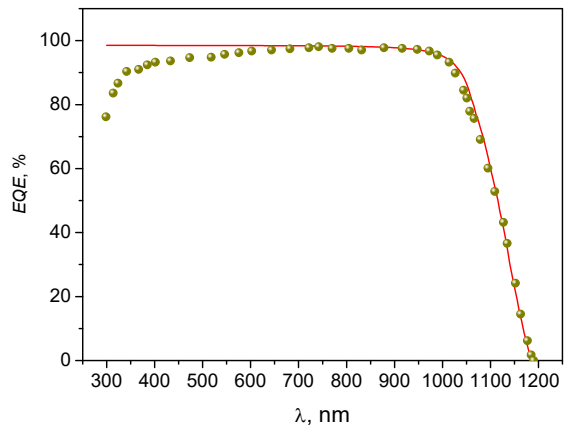


Fig. 1. Experimental spectral dependence of the external quantum efficiency $EQE(\lambda)$ of IBC SC, obtained in [11] (points), while the solid line is the calculation according to formula (2).

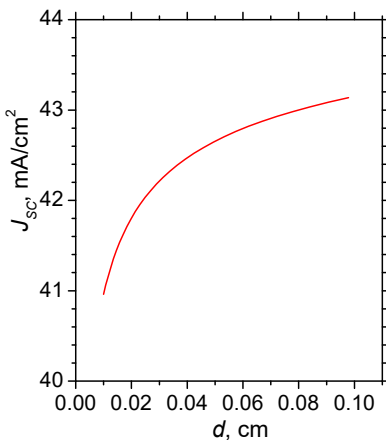


Fig. 2. Calculated dependence of the short-circuit current density on the base thickness d for IBC SC, developed in [11].

E_t – energy of the recombination center, T – temperature, w – thickness of SCR, $L_D = (\epsilon_0 \epsilon_{Si} k T / 2q^2 n_0)^{1/2}$ – Debye length, q – elementary charge, k – Boltzmann constant, ϵ_0 , ϵ_{Si} are the permittivity of free space and relative permittivity of silicon, respectively, y_0 is the non-equilibrium non-dimensional band bending value on the surface of the weakly doped region, which depends on the injection level Δn and is found from the integral neutrality condition, and y_w – non-equilibrium non-dimensional potential on the boundary between the SCR and the quasi-neutral region.

Fig. 3 shows the experimental dependence of the recombination rate in SCR (dots) and its theoretical fit in blue.

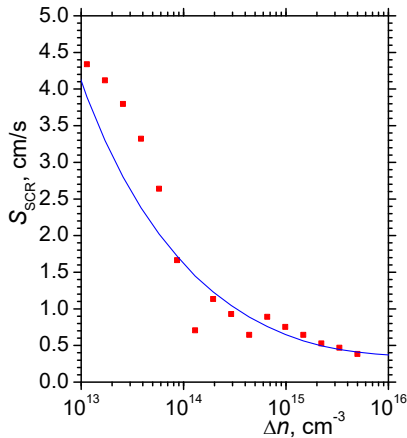


Fig. 3. Recombination rate in SCR as a function of excess concentration. Experiment for SC from [11] (points) and the correlated theoretical fit (solid line). For color interpretation, the reader should be referred to the web version of the journal.

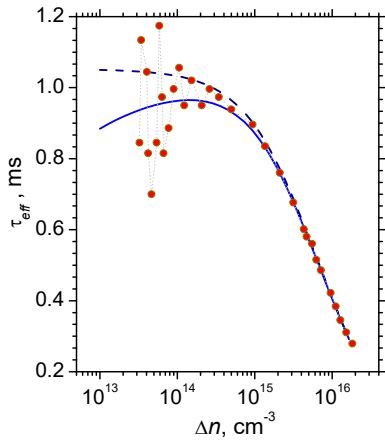


Fig. 4. The excess concentration dependent effective lifetime in the SC base: experiment from [11] (solid circles) and the theoretical (lines). The solid blue line is calculated in the presence of recombination in SCR, while the dashed curve describes the case without recombination.

Fig. 4 shows the experimental dependence of the effective lifetime in the SC base, measured in [11], and corresponding theoretical dependences. Using the recombination rate in the SCR, we can now calculate the theoretical dependence of the effective lifetime on the excess concentration, which is shown in Fig. 4 (solid curve). In the case of a negligibly small recombination rate in the SCR, the dependence of the effective lifetime on the excess concentration is described by the dashed curve shown in Fig. 4. Comparing the last two curves, we can see that in this case the largest difference between them in the region of their maximum values is of the order of 9%, if the value Δn is $1.3 \cdot 10^{14} \text{ cm}^{-3}$ and 15%, when $\Delta n = 1.7 \cdot 10^{13} \text{ cm}^{-3}$. These values are significantly smaller than the difference between the effective lifetime in the presence and absence of recombination in SCR, obtained in [11]. It can be explained by the fact that the

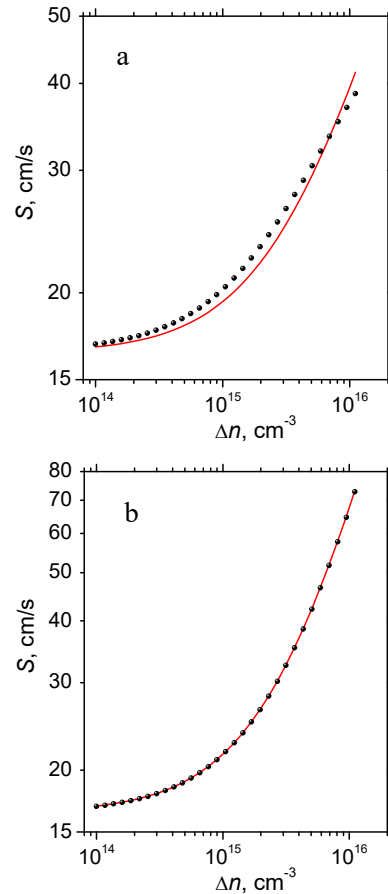


Fig. 5. Dependences of the surface recombination rate S on the excess concentration at the interface between the n and n^+ regions of the SC according Eq. (1) (points) and Eq. (11) (red line) when the charge in the n^+ region $N = -0.515 \cdot 10^{11} \text{ cm}^{-2}$ and the parameter $r = 0.62$ (a) and when the charge in the n^+ region $N = -10^{12} \text{ cm}^{-2}$ and the parameter $r = 1$ (b).

recombination rate in SCR in this case, in the region of actual excess concentration values, is more than an order of magnitude smaller than the surface recombination rate, and in [11], the recombination in SCR is higher than the surface one. This means that in this SC, the recombination in SCR plays a significantly smaller role than in SCs considered in [11].

It is worth noting that the agreement between experimental and theoretical dependence for the effective lifetime in the base (Fig. 4) was obtained when using the coefficient $r = 0.62$ (see Eq. (1)). The introduction explained that this is possible if the charge in the isotype junction is significantly smaller than in the anisotype junction.

Let's prove it. The neutrality equation for the isotype junction is the following:

$$N = -\left(\frac{2kT\epsilon_0\epsilon_{\text{Si}}}{q^2}\right)^{1/2} \left[\frac{(n_0 + \Delta n)(e^y - 1)}{-n_0y + \Delta n(e^{-y} - 1)} \right]^{1/2}, \quad (10)$$

where qN is the surface charge density in the isotype junction. In this case, N is negative.

Fig. 5 shows the dependences of the surface recombination rate for the case when such recombination occurs through a discrete trap level located near the middle of the band gap at the boundary of the n and n^+ regions (defect-assisted SRH recombination). The expression for this recombination rate has the following form:

$$S(\Delta n) = \frac{S_{00}(n_0 + \Delta n)}{(n_0 + \Delta n)e^y + b_r \Delta n e^{-y}}, \quad (11)$$

with $S_{00} = 1/C_{ps}N_{ts}$, where C_{ps} is the hole capture coefficient, N_{ts} is the surface defects level concentration, $b_r = C_{ps}/C_{ns}$, and C_{ns} is the electron capture coefficient.

In the case when $N = -0.515 \cdot 10^{11} \text{ cm}^{-2}$, dependence (11) is in satisfactory agreement with (1) at $r = 0.62$ (see Fig. 5a). If $N = -10^{12} \text{ cm}^{-2}$, then the coefficient r in the dependence $S(\Delta n)$ equals 1 (see Fig. 5b).

4. Modeling of light J–V characteristics and dependences of power on applied voltage for SC [11]

Fig. 6 shows the experimental dependences for light current density-voltage J – V characteristics obtained in [11]. Theoretically, the light J – V characteristic for silicon SCs can be determined from expressions (12)–(15):

$$J_L(V) = J_{SC} - J_r(V) - \frac{V + J_L R_s}{R_{SH}}, \quad (12)$$

$$J_r(V) = qA_{SC} \left(\frac{d}{\tau_{eff}^b} + S_{00} \left(1 + \frac{\Delta n}{n_0} \right) + S_{SCR}^{th} \right) \Delta n(V), \quad (13)$$

$$\tau_{eff}^b(n) = \left[\frac{1}{\tau_{SRH}} + \frac{1}{\tau_{exc}^n(n)} + \frac{1}{\tau_{rad}(n)} + \frac{1}{\tau_{Auger}(n)} \right]^{-1}, \quad (14)$$

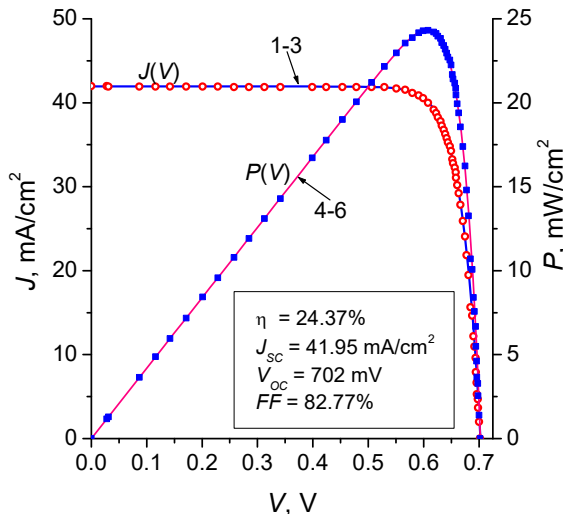


Fig. 6. Light $J(V)$ and $P(V)$ characteristics of SC from [11]. Points are experimentally obtained, and lines (1–3, 4–6) are the theoretical dependences calculated respectively using six-, five- and four-recombination mechanisms. Lines 1–3 and 4–6 visually coincide.

$$\Delta n(V) = -\frac{n_0}{2} + \sqrt{\frac{n_0^2}{4} + n_i(T, \Delta E_g)^2 \left(\exp \frac{q(V + J_L R_s)}{kT} - 1 \right)}, \quad (15)$$

where $J_L(V) = I_L(V)/A_{SC}$ is the total current density, A_{SC} – SC area, J_{SC} – the short-circuit current density, $J_r(V)$ – recombination (dark) current density, V – applied voltage, R_s and R_{SH} are series and shunt resistance, $n = n_0 + \Delta n$ is the total electron concentration in the neutral volume of the base and ΔE_g – temperature-dependent narrowing of the semiconductor band gap.

Fig. 6 also shows theoretical dependences for light J – V characteristics, calculated using approximations of six, five, and four recombination mechanisms. The meaning of the six- and four-mechanism approximations is described above. The case of five mechanisms corresponds to neglecting the recombination in SCR, and with account of non-radiative exciton recombination. The theoretical dependences, shown in Fig. 6, as well as in Fig. 7, were simulated in the following order. Firstly, the dependences were constructed to approximate six recombination parameters, then five and finally, four recombination parameters. As can be seen from Fig. 6, the obtained dependences visually coincide with each other and are consistent with the experiment. The visual coincidence of the dependences here and further in the text means that their deviation is less than 0.1%. In the case of six-recombination approximation the following parameters were used: $S = 14.57 \text{ cm/s}$, $R_s = 0.165 \text{ Ohm}\cdot\text{cm}^2$, $\tau_{SRH} = 7 \cdot 10^{-3} \text{ s}$, $r = 0.62$, $\tau_R = 7 \cdot 10^{-5} \text{ s}$, $b_r = 0.1$, $R_{SH} = 3 \cdot 10^4 \text{ Ohm}\cdot\text{cm}^2$, and $J_{SC} = 41.95 \text{ mA/cm}^2$. In the case of five recombination mechanisms, only the surface recombination rate and the series resistance are changed; therefore, $S = 14.77 \text{ cm/s}$, and $R_s = 0.183 \text{ Ohm}\cdot\text{cm}^2$. When only four mechanisms are considered, the surface recombination rate and series resistance equal $S = 16.1 \text{ cm/s}$, and $R_s = 0.15 \text{ Ohm}\cdot\text{cm}^2$.

The dependence of the SC output power on the applied voltage is described by the expression

$$P(V) = I_L(V)V. \quad (16)$$

Fig. 6 also shows the experimental and theoretical dependences $P(V)$ calculated in the approximations of six, five, and four recombination mechanisms, using the above parameter values. In the case of light J – V characteristics, they coincide with each other. The reason for their coincidence is the insignificance of the recombination in the SCR and non-radiative exciton recombination compared to the surface recombination rate.

The expression for the dark current has the following form:

$$J_D(V) = \frac{qA_{SC}d\Delta n}{\tau_{eff}(\Delta n)} + \frac{V - J_D R_s}{R_{SH}}, \quad (17)$$

$$\Delta n(V) = -\frac{n_0}{2} + \sqrt{\frac{n_0^2}{4} + n_i(T, \Delta E_g)^2 \left(\exp \frac{q(V - J_D R_s)}{kT} - 1 \right)}. \quad (18)$$

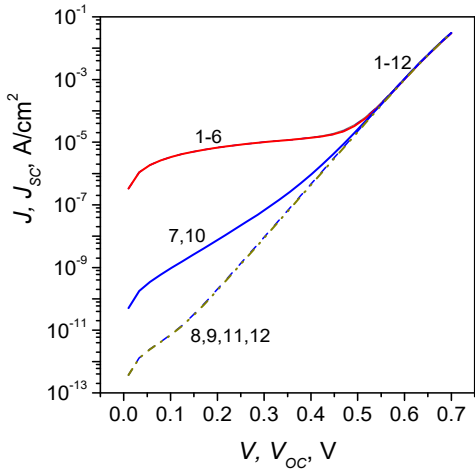


Fig. 7. Theoretical dark J - V characteristics (lines 1–3) and dependences $J_{sc}(V_{oc})$ (lines 4–6), calculated using six (1, 4, 7, 10), five (2, 5, 8, 11) and four (3, 6, 9, 12) recombination mechanisms for the case when the shunt resistance is $3 \cdot 10^4$ (lines 1–6) and $3 \cdot 10^{10}$ Ohm·cm² (lines 7–12). Upper curve contains visually matching lines 1–6, while the middle and lower curves contain similarly matching lines 7, 10 and 8, 9, 11, 12, respectively.

Finally, the dependences of the short-circuit current on the open-circuit voltage are determined from the equations

$$I_{sc}(V_{oc}) = \frac{qA_{sc}d\Delta n_{oc}}{\tau_{eff}(\Delta n_{oc})} + \frac{V_{oc}}{R_{sh}}, \quad (19)$$

$$\Delta n_{oc}(V) = -\frac{n_0}{2} + \sqrt{\frac{n_0^2}{4} + n_i(T, \Delta E_g)^2 \left(\exp \frac{qV_{oc}}{kT} - 1 \right)}. \quad (20)$$

Fig. 7 shows the theoretical dependences for the dark current on the applied voltage and the short-circuit current on the open-circuit voltage in the approximations of four-, five-, and six- recombination mechanisms. In this case, firstly, theoretical dependences for the dark J - V characteristics were calculated and plotted, and then theoretical dependences $J_{sc}(V_{oc})$. In this case, the shunt resistance is relatively small ($3 \cdot 10^4$ Ohm·cm²), and the surface recombination rate significantly exceeds the recombination rate in SCR and the rate of non-radiative exciton recombination. In this case, all the calculated and plotted curves practically coincide visually.

The close similarity of the dark J - V characteristics and the short-circuit current dependences in this case is associated with the small series resistance and the limit of the maximum applied voltage and open-circuit voltage, while the shunt resistance is sufficiently small. It should be noted that with and without the recombination in SCR, the dependences coincide at both low applied voltages and open-circuit voltages only because, in the region of low voltages, the dark current is determined by the shunt resistance. If the shunt resistance is set to be large (about 10^{10} Ohm·cm² or more), then the dark current and the $J_{sc}(V_{oc})$ dependences in the presence and absence of recombination in SCR differ (see Fig. 7).

In this case, as before, theoretical dependences for the dark J - V characteristics were firstly calculated and plotted, and then theoretical dependences $J_{sc}(V_{oc})$.

Consider that most of the simulation programs for calculating key parameters of silicon-based SCs were developed before researchers learned to effectively minimize surface recombination. Therefore, it becomes clear why the theoretical dependences obtained in the approximation of four recombination mechanisms were in good agreement with the experiment. The situation changed when technologies were developed for effective passivation of the surface of silicon crystals, which reduced the surface recombination to a few cm/s or even less [12, 21–25]. As the results of our studies, in [10, 27], have shown that in cases where surface recombination is less than recombination in SCR, the latter should be considered. In this case, recombination in SCR has a particularly strong influence on the dependence of the effective lifetime on excess concentration.

5. Optimization of the parameters of SC studied in [11]

In the case described in [10], the efficiency obtained in [11] can be increased by optimizing the base thickness and the base doping level. Our calculations showed that the maximum efficiency of 24.62% can be achieved at the base doping level of $5 \cdot 10^{15}$ cm⁻³ and the thickness of 520 μm. The dependence of the output power of the optimized SC on the applied voltage for this case is shown in Fig. 8. Considering that the experimental efficiency from [11] was 24.37%, the authors of the work have selected parameters that allowed getting the efficiency close to the optimal one.

Fig. 9 plots the dependences of the photoconversion efficiency on the surface recombination rate. One can see that at $S \geq 20$ cm/s, the values of the photoconversion efficiency calculated in the approximations of six and

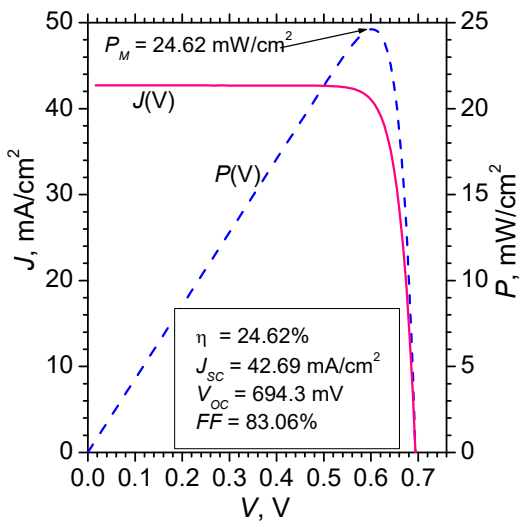


Fig. 8. Theoretical light $J(V)$ and $P(V)$ characteristics of the optimized SC, calculated using the six recombination mechanisms approach.

four recombination mechanisms visually coincide. It is also seen that even at $S = 100 \text{ cm/s}$, the photoconversion efficiency remains sufficiently high.

6. Modeling of light I - V characteristics and dependences of useful power on excess concentration for work [17]

Fig. 10 shows the experimental dependences for the light J - V characteristics from [17], as well as the theoretical ones in the approximations of six and four recombination mechanisms. The calculated graphs use the formalism from [18] with the following parameters: $\tau_m = 3.8 \cdot 10^{-6} \text{ s}$, $x_m = 8.5 \cdot 10^{-6} \text{ cm}$, $\sigma = 2.4 \cdot 10^{-6} \text{ cm}$, $b_r = 0.1$, $\tau_{SRH} = 2.1 \cdot 10^{-3} \text{ s}$, $S_0 = 17.4 \text{ cm/s}$, $R_S = 0.64 \text{ Ohm} \cdot \text{cm}^2$, where τ_m is the lifetime at the maximum point, x_m is the position of the maximum, and σ is the dispersion of Gauss distribution.

As can be seen from the figure, the voltage-dependent light $J(V)$ characteristics, calculated in the approximations of six and four mechanisms, visually coincide.

Fig. 10 also shows the experimental dependence of the output power on the applied voltage $P(V)$ and the theoretical dependences in the approximations of six and four recombination mechanisms, calculated following the approach of [18]. As can be seen from the figure, the theoretical dependences of the output power, calculated in the approximations of six and four recombination mechanisms, also coincide.

In this case, the excess concentration at the maximum efficiency point is $1.96 \cdot 10^{14} \text{ cm}^{-3}$, $S = 18.1 \text{ cm/s}$, $S_{SCR} = 9.6 \text{ cm/s}$. Thus, in contrast to [11], the surface recombination and recombination rates in SCR are comparable. However, in the case of four recombination mechanisms, when recombination in SCR is absent, it is necessary to consider the change in the surface recombination rate to reconcile theoretical dependences with the experimental ones. This consideration gives a new surface recombination rate, with its 26.6 cm/s minimum value. From the comparison of the total surface

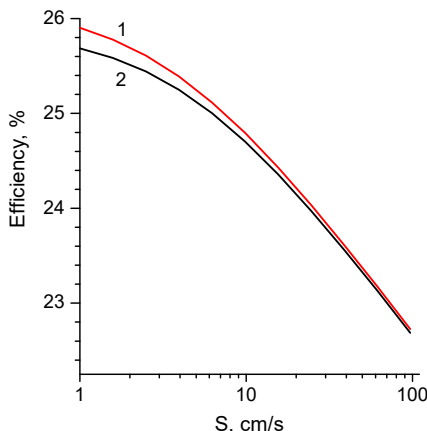


Fig. 9. Dependence of the efficiency of SC photoconversion on the rate of surface recombination at the boundary of the isotype junction calculated using approaches with four (1) and six (2) recombination mechanisms.

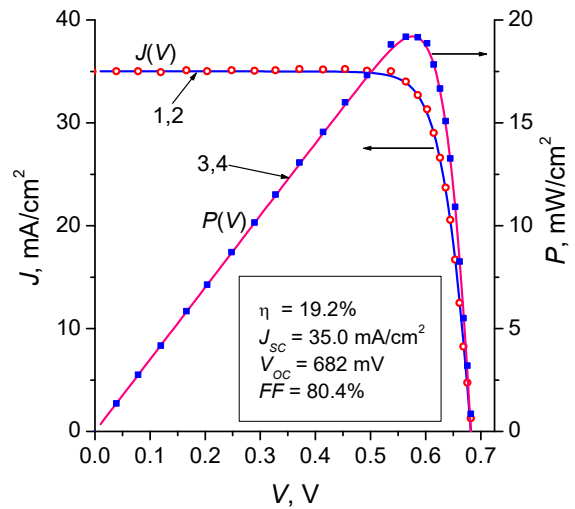


Fig. 10. Light $J(V)$ and $P(V)$ characteristics of the SC from [17]. Points are experiments, and lines are the theoretical dependences calculated, respectively, using six (lines 1, 3), and four (lines 2, 4) recombination mechanisms. Lines 1, 2 and 3, 4 visually coincide.

recombination rate and recombination rate in SCR and the new surface recombination rate, it is seen that at the point of maximum power, they are the same. This explains the coincidence of theoretical dependences in the case of six and four mechanisms.

7. Conclusions

In summary, as shown experimentally in [11] and explained in this paper, a sufficiently high efficiency exceeding 24% can be obtained even when the surface recombination rate is sufficiently high. This is due to the high-quality texturing, which results in a short-circuit current density of the order of 42 mA/cm^2 .

We have shown that for SC studied in [11] the exponential index r in expression (1) for the surface recombination rate on the excess concentration is 0.62, which is less than unity – the value that usually occurs. We explain this by the fact that in this case, the donor charge in the isotype contact is much smaller than the acceptor charge in the anisotropic contact.

It was also shown that for the theoretical modeling of the light J - V characteristics, dark J - V characteristics, short-circuit current, and output power, the approximation of four recombination mechanisms can be used. This can be done when the surface recombination rate significantly exceeds both the recombination rate in the SCR and the rate of non-radiative exciton recombination.

The corresponding criteria that allow using the approximation of the four recombination mechanisms for modeling SCs are satisfied for SCs in experimental works [11, 17]. At the same time, when calculating the effective lifetime, it is always necessary to consider the recombination in SCR; otherwise, there is no region of decreasing $\tau_{eff}(\Delta n)$ with decreasing Δn at a small Δn .

References

1. Oni A.M., Mohsin Abu S.M., Rahman Md.M., Bhuiyan M.B.H. A comprehensive evaluation of solar cell technologies, associated loss mechanisms, and efficiency enhancement strategies for photovoltaic cells. *Energy Rept.* 2024. **11**. P. 3345–3366. <https://doi.org/10.1016/j.egyr.2024.03.007>.
2. Mdallal A., Yasin A., Mahmoud M. *et al.* A comprehensive review on solar photovoltaics: Navigating generational shifts, innovations, and sustainability. *Sustainable Horizons*. 2025. **13**. P. 100137. <https://doi.org/10.1016/j.horiz.2025.100137>.
3. Liu Y., Li Y., Wu Y. *et al.* High-efficiency silicon heterojunction solar cells: Materials, devices and applications. *Mater. Sci. Eng.: R: Rep.* 2020. **142**. P. 100579. <https://doi.org/10.1016/j.mser.2020.100579>.
4. Ballif C., Haug F.-J., Boccard M. *et al.* Status and perspectives of crystalline silicon photovoltaics in research and industry. *Nat. Rev. Mater.* 2022. **7**, No 8. P. 597–616. <https://doi.org/10.1038/s41578-022-00423-2>.
5. Philipps S. Photovoltaics report, Fraunhofer Institute for Solar Energy Systems. Freiburg, July 29, 2024. URL: www.ise.fraunhofer.de/en/publications/studies/photovoltaics-report.html (Last accessed: 15.05.2025).
6. Green M.A., Dunlop E.D., Yoshita M. *et al.* Solar cell efficiency tables (version 64). *Prog. Photovolt.: Res. Appl.* 2024. **32**. P. 425–441. <https://doi.org/10.1002/pip.3831>.
7. Sachenko A., Kostylyov V., Sokolovsky I., Evstigneev M. Effect of temperature on limit photoconversion efficiency in silicon solar cells. *IEEE J. Photovolt.* 2020. **10**. P. 63–69. <https://doi.org/10.1109/JPHOTOV.2019.2949418>.
8. Engelbrecht D., Tiedje T. Temperature and intensity dependence of the limiting efficiency of silicon solar cells. *IEEE J. Photovolt.* 2021. **11**. P. 73–84. <https://doi.org/10.1109/JPHOTOV.2020.3035115>.
9. Niewelt T., Steinhauser B., Richter A. *et al.* Reassessment of the intrinsic bulk recombination in crystalline silicon. *Sol. Energy Mater. Sol. Cells.* 2022. **235**. P. 111467(1–13). <https://doi.org/10.1016/j.solmat.2021.111467>.
10. Kostylyov V.P., Sachenko A.V., Evstigneev M. *et al.* Characterization and optimization of high-efficiency crystalline silicon solar cells: Impact of recombination in the space charge region and trap-assisted Auger exciton recombination. *J. Appl. Phys.* 2025. **137**. P. 023101. <https://doi.org/10.1063/5.0239369>.
11. Franklin E., Fong K., McIntosh K. *et al.* Design, fabrication and characterization of a 24.4% efficient interdigitated back contact solar cell. *Prog. Photovolt.: Res. Appl.* 2014. **24**, No 4. P. 411–427. Special Issue: 29th EU PVSEC in Amsterdam, The Netherlands, 2014. <https://doi.org/10.1002/pip.2556>.
12. Lin H., Yang M., Ru X. *et al.* Silicon heterojunction solar cells with up to 26.81% efficiency achieved by electrically optimized nanocrystalline-silicon hole contact layers. *Nat. Energy.* 2023. **8**. P. 789–799. <https://doi.org/10.1038/s41560-023-01255-2>.
13. Taguchi M., Yano A., Tohoda S. *et al.* 24.7% record efficiency hit solar cell on thin silicon wafer. *IEEE J. Photovolt.* 2014. **4**. P. 96–99. <https://doi.org/10.1109/JPHOTOV.2013.2282737>.
14. Yamamoto K., Yoshikawa K., Uzu H., Adachi D. High-efficiency heterojunction crystalline Si solar cells. *Jpn. J. Appl. Phys.* 2018. **57**. P. 08RB20(1–8). <https://doi.org/10.7567/JJAP.57.08RB20>.
15. Richter A., Benick J., Feldmann F. *et al.* *n*-Type Si solar cells with passivating electron contact: Identifying sources for efficiency limitations by wafer thickness and resistivity variation. *Sol. Energy Mater. Sol. Cells.* 2017. **173**. P. 96–105. <https://doi.org/10.1016/j.solmat.2017.05.042>.
16. Yoshikawa K., Yoshida W., Irie T. *et al.* Exceeding conversion efficiency of 26% by heterojunction interdigitated back contact solar cell with thin film Si technology. *Sol. Energy Mater. Sol. Cells.* 2017. **173**. P.37–42. <https://doi.org/10.1016/j.solmat.2017.06.024>.
17. Zin N., Blakers A., McIntosh K. *et al.* 19% Efficient *n*-type all-back-contact silicon wafer solar cells with planar front surface. *Proc. 49th Australian Solar Energy Society's (AuSES) Conf.*, Sydney, Australia, Nov. 30 – Dec. 2, 2011.
18. Sachenko A., Kostylyov V., Vlasiuk V. *et al.* Modeling of the key characteristics of high-efficiency silicon solar cells with planar surfaces, 2021 IEEE 48th Photovoltaic Specialists Conference (PVSC), Fort Lauderdale, FL, USA, 2021. P. 0590–0595. <https://doi.org/10.1109/PVSC43889.2021.9518502>.
19. Sai H., Oku T., Sato Y. *et al.* Potential of very thin and high efficiency silicon heterojunction solar cells. *Prog. Photovolt. Res. Appl.* 2019. **27**. P. 1061–1070. <https://doi.org/10.1002/pip.3181>.
20. Tiedje T., Yablonovitch E., Cody G.D., Brooks B.J. Limiting efficiency of silicon solar cells. *IEEE Trans. Electron. Devices.* 1984. **31**, No 5. P. 711–716. <https://doi.org/10.1109/T-ED.1984.21594>.
21. Hermle M., Feldmann F., Bivour M. *et al.* Passivating contacts and tandem concepts: Approaches for the highest silicon-based solar cell efficiencies. *Appl. Phys. Rev.* 2020. **7**, No 2. P. 21305. <https://doi.org/10.1063/5.0239369>.
22. Richter A., Müller R., Benick J. *et al.* Design rules for high-efficiency both-sides-contacted silicon solar cells with balanced charge carrier transport and recombination losses. *Nat. Energy.* 2021. **6**, No 4. P. 429–438. <https://doi.org/10.1038/s41560-021-00805-w>.
23. Glunz S.W., Steinhauser B., Polzin J.-I. *et al.* Silicon-based passivating contacts: the TOPCon route. *Prog. Photovolt. Res. Appl.* 2023. **31**. P. 341. <https://doi.org/10.1002/pip.3522>.
24. Yan D., Cuevas A., Stuckelberger J. *et al.* Silicon solar cells with passivating contacts: Classification and performance. *Prog. Photovolt. Res. Appl.* 2023. **31**, No 4. P. 310–326. <https://doi.org/10.1002/pip.3574>.
25. Basnet R., Yan D., Kang D. *et al.* Current status and challenges for hole-selective poly-silicon based passivating contacts. *Appl. Phys. Rev.* 2024. **11**. P. 011311. <https://doi.org/10.1063/5.0185379>.

26. Sachenko A.V., Kostylyov V.P., Evstigneev M. Space charge region recombination in highly efficient silicon solar cells. *SPQEO*. 2024. **27**, No 1. P. 10–27. <https://doi.org/10.15407/spqeo27.01.010>.

Authors' contributions

- Sachenko A.V.:** formulation of the problem, analysis, investigation, data curation (partially), writing – original draft, writing – review & editing.
- Kostylyov V.P.:** conceptualization, methodology, analysis, validation, data curation, writing – original draft, writing – review & editing.
- Sokolovskyi I.O.:** theoretical investigation, resources, software.
- Shkrebtii/Chkrebtii A.I.:** analysis, validation, resources, writing – review & editing.

Authors and CV



Sachenko A.V. Professor, Doctor of Physics and Mathematics Sciences, Chief Researcher at the Laboratory of Physical and Technical Fundamentals of Semiconductor Photovoltaics at the V. Lashkaryov Institute of Semiconductor Physics. Author of more than 300 scientific publications.

His main research interests include analysis, characterization, and modeling of silicon solar cells. <https://orcid.org/0000-0003-0170-7625>



Kostylyov V.P. Professor, Doctor of Physics and Mathematics Sciences, Head of the Solar Cell and Solar Module Testing Center, V. Lashkaryov Institute of Semiconductor Physics. Author of over 300 scientific publications. The area of his scientific interests includes photovoltaics and betavoltaics, research, analysis and modeling of solar cells, testing the solar cells and characterization of the optical and recombination properties of photovoltaics materials. <https://orcid.org/0000-0002-1800-9471>



Sokolovskyi I.O. PhD, Senior Researcher of the Laboratory of Physical and Technical Fundamentals of Semiconductor Photovoltaics at the V. Lashkaryov Institute of Semiconductor Physics. Author of more than 70 scientific publications. His main research interests include modeling of silicon solar cells. E-mail: i.o.sokolovskyi@gmail.com, <https://orcid.org/0000-0002-7072-6670>



Shkrebtii/Chkrebtii A.I. Professor at the Ontario Tech University. His recent focus is on hydrogenbonding, nanomaterials hydrogenation, ubiquitous in physical, chemical and biological sciences. E-mail: Anatoli.Chkrebtii@ontariotechu.ca, <https://orcid.org/0000-0002-4998-1538>

Особливості характеризації та оптимізації високоекспективних кремнієвих сонячних елементів, в яких домінує поверхнева рекомбінація

А.В. Саченко, В.П. Костильов, І.О. Соколовський, А.І. Шкrebтii

Анотація. У роботі досліджено особливості моделювання процесів фотоперетворення у високоекспективних сонячних елементах (СЕ) на основі монокристалічного кремнію для випадку, коли внесок поверхневої рекомбінації значно переважає внески рекомбінації в області просторового заряду (ОПЗ) та безвипромінювальної екситонної рекомбінації за участю домішкових центрів. Показано, що в цьому випадку ключові характеристики процесу фотоперетворення, а саме темнова і світлова вольт-амперні характеристики та залежності вихідної потужності СЕ, отримані з урахуванням та без урахування рекомбінації в ОПЗ та безвипромінювальної екситонної рекомбінації за участю домішкових центрів, практично збігаються між собою. Результати моделювання порівнювалися з експериментом для СЕ з двох робіт, в яких мали місце зазначені вище умови. Аналіз підтверджив узгодженість теоретичних залежностей, отриманих з урахуванням та без урахування рекомбінації в ОПЗ та безвипромінювальної екситонної рекомбінації, з експериментальними даними. Показано, що оптимізація рівня легування бази та товщини досліджуваного сонячного елемента приводить до збільшення його ефективності з 24,37% до 24,62%. Результати, отримані в роботі, дозволяють пояснити, чому раніше рекомбінація в ОПЗ не враховувалася при теоретичному моделюванні характеристик СЕ на основі монокристалічного кремнію у переважній кількості робіт, а також показати, що загальний підхід справедливий у випадку будь-якого співвідношення між компонентами струмів рекомбінації в монокристалічному кремнії.

Ключові слова: моделювання, кремнієвий сонячний елемент, швидкість поверхневої рекомбінації, рекомбінація в ОПЗ, ефективність фотоперетворення.